Exploring the dynamic rotational profile of the hotter solar atmosphere: A multi-wavelength approach using SDO/AIA data

Srinjana Routh [ID],[1,2] Bibhuti Kumar Jha [ID],[3] Dibya Kirti Mishra [ID],[1,2] Tom Van Doorsselaere [ID],[4]
Vaibhav Pant [ID],[1] Subhamoy Chatterjee [ID],[3] and Dipankar Banerjee [ID][1,5,6]

[1] Aryabhatta Research Institute of Observational Sciences, Nainital-263002, Uttarakhand, India
[2] Mahatma Jyotiba Phule Rohilkhand University, Bareilly-243006, Uttar Pradesh, India
[3] Southwest Research Institute, Boulder, CO 80302, USA
[4] Centre for mathematical Plasma Astrophysics, Mathematics Department, KU Leuven, Celestijnenlaan 200B
bus 2400, B-3001 Leuven, Belgium
[5] Indian Institute of Astrophysics, Koramangala, Bangalore 560034, India
[6] Center of Excellence in Space Sciences India, IISER Kolkata, Mohanpur 741246, West Bengal, India

ABSTRACT

Understanding the global rotational profile of the solar atmosphere and its variation is fundamental to uncovering a comprehensive understanding of the dynamics of the solar magnetic field and the extent of coupling between different layers of the Sun. In this study, we employ the method of image correlation to analyze the extensive dataset provided by the Atmospheric Imaging Assembly of the Solar Dynamic Observatory in different wavelength channels. We find a significant increase in the equatorial rotational rate (A) and a decrease in absolute latitudinal gradient ($|B|$) at all temperatures representative of the solar atmosphere, implying an equatorial rotation up to 4.18% and 1.92% faster and less differential when compared to the rotation rates for the underlying photosphere derived from Doppler measurement and sunspots respectively. In addition, we also find a significant increase in equatorial rotation rate (A) and a decrease in differential nature ($|B|$ decreases) at different layers of the solar atmosphere. We also explore a possible connection from the solar interior to the atmosphere and interestingly found that A at $r = 0.94\,\mathrm{R}_\odot, 0.965\,\mathrm{R}_\odot$ show an excellent match with 171 Å, 304 Å and 1600 Å, respectively. Furthermore, we observe a positive correlation between the rotational parameters measured from 1600 Å, 131 Å, 193 Å and 211 Å with the yearly averaged sunspot number, suggesting a potential dependence of the solar rotation on the appearance of magnetic structures related to the solar cycle or the presence of cycle dependence of solar rotation in the solar atmosphere.

1. INTRODUCTION

Rotation is a fundamental aspect in the pursuit of a comprehensive understanding of our nearest star, the Sun. The study of solar rotation has been a persistent topic in solar physics since the 17th century and has become increasingly important in recent years due to its strong connection with the solar magnetic field (Parker 1955a,b; Charbonneau 2010). Early studies on the differential rotation in the photosphere of the Sun

Corresponding author: Dipankar Banerjee
dipu@aries.res.in

relied on tracking of prominent photospheric magnetic features called sunspots (Carrington 1859; Newton & Nunn 1951), which allowed for the measurement of photospheric differential rotation in the form of (Weber 1999),

$$\Omega = A + B\sin^2\theta + C\sin^4\theta, \qquad (1)$$

where θ is the latitude, A is the equatorial rotation rate, and B and C are the coefficients of a quadratic expansion in $\sin^2\theta$, often physically interpreted as latitudinal gradients (Li et al. 2013).

In the past century, advances in measuring techniques and instruments have significantly improved the accuracy of sunspot tracking (Ward 1966; Balthasar et al.

1986; Gupta et al. 1999; Javaraiah et al. 2005; Jha et al. 2021; Jha 2022), and have also led to the development of new measurement techniques such as spectroscopy (Howard & Harvey 1970; Howard et al. 1984; Snodgrass 1984; Snodgrass et al. 1990; Vats et al. 2001). Furthermore, extensive research, in conjunction with the more recent field of helioseismology (Antia et al. 1998; Komm et al. 2008; Howe 2009), has enabled us to gain a comprehensive understanding of the rotational profile of the Sun till photosphere, including its variations with depth. However, a complete understanding of the rotational profile of the Sun above the photosphere and its variation with temperature (or height) remains elusive.

Initial investigations into the rotational profile of the higher solar atmosphere, where magnetic field dominates the dynamics (Stix 1976; Gary 2001; Rodríguez Gómez et al. 2019), suggested a faster rate of rotation than the photosphere (Hale 1908; Evershed 1925; Aslanov 1964; Hansen et al. 1969; Livingston 1969). These findings were contradicted by the subsequent studies that suggested a rotational profile of different parts of the solar atmosphere to be similar to that of the photosphere or sunspots, if not even slower (Fisher & Sime 1984; Brajša et al. 1999, 2004; Bertello et al. 2020). Studies also made efforts to utilise higher atmospheric features like filaments (Glackin et al. 1974; Brajša et al. 1991; Japaridze et al. 1992); coronal bright points (CBPs; Brajša et al. 2004; Sudar et al. 2015); coronal streamers (Morgan 2011; Edwards et al. 2022); magnetic loops (e.g., Pneuman et al. 1971); coronograph images (e.g., Lewis et al. 1999; Mancuso et al. 2020); Ca^+ network and plages (e.g., Schröter et al. 1978; Bertello et al. 2020; Mishra et al. 2024); soft X-ray observation (SXR; Chandra et al. 2010), wavelength bands like 171 Å, 193 Å, 304 Å, etc. (Sharma et al. 2020; Sharma et al. 2021) and radio flux information (e.g., Vats et al. 2001; Bhatt et al. 2017) to obtain the rotational profile of the different layers of hotter solar atmosphere. Additionally, some studies reported an increase in rotation rate with temperature/height (e.g., Adams & Tang 1977; Vats et al. 2001; Sharma et al. 2020), while others found contrary results (e.g., Bhatt et al. 2017; Badalyan & Obridko 2018). These studies used various methods, including the tracer method (e.g, Schröter et al. 1978), periodogram (e.g, Weber et al. 1999), auto-correlation(e.g., Sharma et al. 2020; Sharma et al. 2021) and cross-correlation method (e.g., Bertello et al. 2020; Mishra et al. 2024) to obtain diverse results, which have been unable to resolve the problem of atmospheric solar rotation, persisted for over a century.

Studies akin to that of Glackin et al. (1974); Ternullo (1986); Japaridze et al. (1992); Komm et al. (1993a)

have linked the cause of these reported differences in the obtained rotational profiles based on the nature of the tracer chosen. However, other studies, such as those by Altrock (2003); Mishra et al. (2024) attributed the probable cause to the characteristics of the data selected for analysis. Additionally, several studies have also explored the correlation between the solar cycle and the rotational profile of the solar corona and transition region (Sime et al. 1989; Komm et al. 1993a; Imada et al. 2020; Sharma et al. 2021; Edwards et al. 2022; Zhang et al. 2023) in a pursuit to explore the role of solar magnetic activity in driving the rotation of the solar atmosphere. The reported link in their respective findings suggests a cyclic behaviour in equatorial rotation and a differential nature in these layers, similar to the solar cycle but with a lag (Sharma et al. 2021; Zhang et al. 2023). But such a pursuit was too riddled with further contradictions as other studies (e.g., Li et al. 2012; Bertello et al. 2020; Mishra et al. 2024) reported finding no such significant variation in the rotation rate of the solar chromosphere (Mishra et al. 2024) and corona with the solar cycle. The contrasting findings from these studies have been explored through various theoretical and analytical perspectives. Among those perspectives, the potential connection between the solar interior and the solar atmosphere through magnetic fields has been consistently proposed in many studies to resolve some of these perplexing results (e.g. Weber 1969; Wang et al. 1989; Badalyan & Sýkora 2005; Bagashvili et al. 2017; Finley & Brun 2023).

Despite utilizing various methods and datasets, a comprehensive understanding of the global rotational profile of the solar atmosphere above the photosphere and how it varies across different layers remains elusive due to the diverse results obtained. In an attempt to address this gap, this study adopts a more focused approach by utilizing a single tracer-independent method, that is, the method of image correlation, to analyze the extensive dataset provided by the Atmospheric Imaging Assembly (AIA) of the solar Dynamic Observatory (SDO) from the period of 2010–2023. Additionally, we utilize the internal rotation rates derived using helioseismology from Antia et al. (1998, 2008), photospheric rotation rate using sunspot (Jha et al. 2021), and chromospheric rotation rate using chromospheric plage (Mishra et al. 2024), to connect the global variation of the solar differential rotation profile from subsurface regime to the atmosphere. In section 2, we will discuss the specific details of the dataset used; section 3 will discuss the modifications made to the method initially proposed by Mishra et al. (2024) for this study before moving on to section 4 and section 5 where results obtained from the

analysis will be discussed. The final section 6 will summarize the study and highlight its key conclusions.

2. DATA

The Atmospheric Imaging Assembly (AIA; Lemen et al. 2012) on the Solar Dynamics Observatory (SDO; Chamberlin et al. 2012; Pesnell et al. 2012) captures data across multiple extreme ultraviolet (EUV) and ultraviolet (UV) wavelengths. By employing narrow-band imaging in ten specific temperature-sensitive wavelength channels, such as Fe XVIII (94 Å), Fe VIII, XXI (131 Å), Fe IX (171 Å), Fe XII, XXIV (193 Å), Fe XIV (211 Å), He II (304 Å), and Fe XVI (335 Å), the AIA probes the solar atmosphere at different temperatures ranging from $\approx 10^4$ K to 10^7 K. The AIA observes regions of solar atmosphere starting from the photosphere and above, extending through the chromosphere, transition region, and lower corona, with a pixel scale of $0.6''$/pixel. In addition, one of the telescopes of the AIA observes in C IV line near 1600 Å and the nearby continuum at 1700 Å as well as in the visible continuum at 4500 Å (Lemen et al. 2012). The AIA has been providing data from May 2010 to the present, covering solar cycle 24 and ongoing cycle 25.

For this study, we primarily utilize data from seven different wavelength channels, namely 1600 Å, 304 Å, 131 Å, 171 Å, 193 Å, 211 Å and 335 Å from the period of 2010–05–13 to 2023–08–30 at a cadence of 6 hours. This was done to ensure that only features with a lifespan longer than 6 hours contributed to the analysis while still providing sufficient data for robust statistical analysis. The 94 Å band was excluded from the analysis due to its poor signal-to-noise ratio in the low-temperature regime (Aschwanden et al. 2013; Nuevo et al. 2015). The initial dataset, classified as Level 1, is obtained from the Joint Science Operations Center[1] (JSOC; Hapgood et al. 1997) and converted to level 1.5 using Interactive Data Language (IDL) version of *aia_prep.pro*, available under AIA/SolarSoft (Freeland & Handy 1998). This step aligns the solar north with that of the image and applies the necessary adjustments required to make the plate scale consistent across all wavelength bands (Lemen et al. 2012). This Level 1.5 data from 2010–05-13 to 2023–08–30 was used to get the rotation profile of the Sun across all the aforementioned wavelengths.

3. METHODOLOGY

3.1. *Pre-Processing*

The hotter solar atmosphere is ubiquitously populated with small-scale features that are often short-lived and can undergo significant changes within a very short span of time (Solanki 1993; Bhatnagar & Livingston 2005). Since the method of image correlation depends only on pixel-specific intensities in consecutive images, such rapid changes in the small-scale structures negatively affect the correlation coefficient, thereby affecting our analyses. Therefore, the data was smoothed by convolving them with a Gaussian kernel to remove such small scale features to minimize the contribution from them. The size of the Gaussian kernel ($\sigma = 5''$) was chosen keeping in mind the angular size of the small-scale features ($\Delta\theta \approx 1''$- $5''$ e.g., chromospheric network and internetwork, quiet Sun concentrations; Pozuelo et al. 2023). Additionally, this procedure serves as a step to minimize the random noise and help us to improve the signal-to-noise ratio of large-scale structures (Chung 2012), see Figure 1 for a representative example.
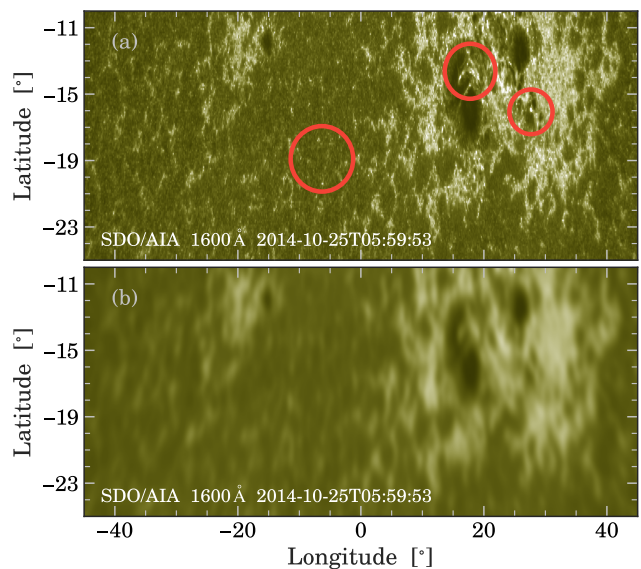

Figure 1. An example pair of images showing the effectiveness of Gaussian smoothing. (a) The level 1.5 data from 1600 Å with small scale brightenings, network bright points and fracture in plage regions. (b) The data after smoothing, as a result of convolution with a Gaussian kernel.

3.2. *Method of Image Correlation*

After applying a Gaussian smoothing filter, we utilized the image correlation technique similar to Mishra et al. (2024) to determine the rotation rate in different latitude bands. The image correlation method utilizes the two-dimensional (2D) cross-correlation technique to determine the offset between two images. This method has been previously suggested to focus on the rotation of the magnetic features as has been discussed in Snodgrass (1983, 1992) and Stenflo (1989). The method is

---

[1] AIA data can be downloaded from here

briefly outlined below, but for a detailed discussion, the reader is encouraged to refer to Mishra et al. (2024).

We project the full-disk AIA data to a heliographic grid of size 1800 pixels × 1800 pixels (0.1°/pixel in latitude and longitude) using the near-point interpolation; see Figure 2(a), similar to the process demonstrated in Mishra et al. (2024). These projected images are then divided into overlapping bins of 15°, each separated by a 5° stride e.g., 0° − 15°, 5° − 20° etc. (see Figure 2). The choice of 15° bin is made to minimize the impact of any partially remaining extended features (Weber et al. 1999; Meunier & Leweke 2003; Riha et al. 2007) and improve the cross-correlation coefficient. Furthermore, the overlapping bins are chosen to ensure a sufficient number of latitudinal bands were probed. These bins are selected over the span of ±60° (in the case of 171 Å, 193 Å, and 211 Å), ±55° (in the case of 1600 Å, 304 Å) and ±45° (in the case of 335 Å and 131 Å) in latitude (θ) and ±45° in longitude (ϕ). These multiple latitudinal extents are selected to take into account the presence of most of the large-scale features across different wavelength channels e.g., active regions, large-scale coronal bright points (CBPs) within ±45°, plages within ±55°. Additionally, these limits also serve to reduce the projection effects at higher latitudes ($\theta > \pm60°$) and near the limb (Weber et al. 1999; Deforest 2004). The latitude of the bin is assigned as the centre of the selected bin, e.g., for 0° − 15° it is 7.5°. Subsequently, two bins (say B1 and B2) of the same latitudinal extent from consecutive images (separated by 6 hrs in time) are used to calculate the 2D cross-correlation function by shifting B2 with respect to B1 for the set of $\Delta\phi \in [\phi_0 − 3°, \phi_0 + 3°]$ in longitude and $\Delta\theta \in [\theta_0 − 1°, \theta_0 + 1°]$ in latitude direction, where ϕ_0 is the expected longitudinal shift estimated based on the photospheric rotation rate (Jha et al. 2021) and θ_0 is taken as 0. Finally, the $\Delta\phi$ and $\Delta\theta$ are identified by maximizing the 2D cross-correlation function[2]. Since this study is focused towards the measurement of differential rotation particularly, only the value of $\Delta\phi$ was used to calculate the value of Ω in that latitudinal bin.

4. RESULTS

4.1. Average rotational profile above the photosphere

To obtain the average rotational profile of the hotter solar atmosphere above the solar photosphere, we calculated the average of $\Omega(\theta)$ for each latitudinal band weighted by corresponding cross-correlation coefficients
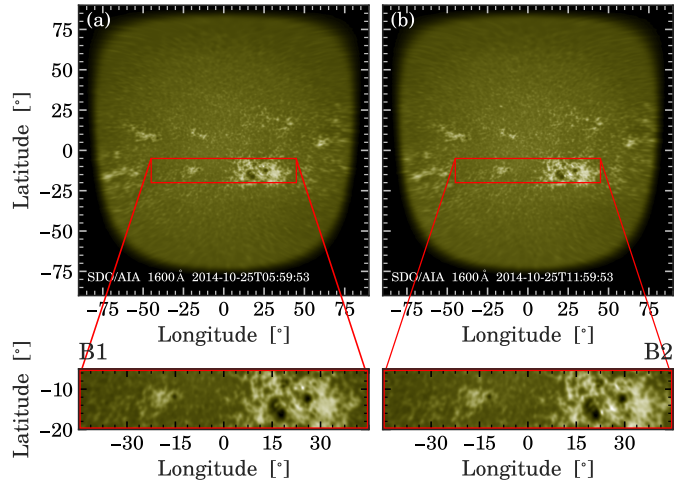
---

[2] The image cross-correlation was performed using correl_images.pro and corrmat_analyze.pro routines available in the Solar SoftWare library.

Figure 2. Panels (a) and (b) depict an example pair of images, temporally separated by 6 hours, after projection onto the heliographic grid. Red rectangular boxes in (a) and (b) represent the selected bands (B1 and B2) for cross-correlation, spanning −20° to −5°) in latitude and ±45° in longitude in this example.

(CC) in that latitude band. This step is performed after the elimination of cases with low values of CC, which may have arisen due to the absence or emergence of any large-scale feature in either of the consecutive images being analyzed. Low values of CC may also result from the presence of transient events (e.g., flares), which lead to intensity enhancements in any of the consecutive images being correlated. Cases where CC < 0.65 for 131 Å, 171 Å, 193 Å, 211 Å, 335 Å and CC < 0.70 for 304 Å and 1600 Å are not included in analysis. These limits on the CC are imposed after finding out the value of CC for which the values of A, B and C do not vary significantly (for detailed discussion on this approach see Mishra et al. 2024). The uncertainty (error) in Ω_θ is calculated as the resultant of the least count error (σ_{LCE}) and the standard statistical error (σ_{SSE}) of the mean. However, σ_{LCE} remains dominant in the total error estimate[3], as σ_{LCE} is an order of magnitude greater than the σ_{SSE} (shaded region of respective colours for each wavelength band in Figure 3). The values of mean Ω_θ thus obtained for each latitudinal bin are then fitted with Equation 1 (where $\theta = \theta_{mid}$ is the centre of the latitude band) using the least square fit method, to obtain the best-fit parameters (A, B, C) and their associated uncertainties (ΔA, ΔB, ΔC). These steps are repeated for each AIA wavelength channel, and the differential

---

[3] $\sigma_{\mathrm{LCE}} = \frac{\Delta\phi}{\Delta t} = \frac{0.1°}{0.25\,\mathrm{days}} = 0.4°$

rotation parameters obtained are tabulated in Table 1 for the same.

Our first interpretation from Figure 3 is that the rotation profile in the solar atmosphere, from the upper photosphere to the corona, exhibits a similar rotational profile across all wavelengths. However, the rotational profile is relatively flatter i.e less differential whereas the absolute rotation rate is higher compared to the photosphere, as observed using Dopplergrams (olive green dash-dotted line in Figure 3; Snodgrass 1984; Ulrich & Bertello 1996) and sunspots as tracers (dark grey dotted line in Figure 3; Jha et al. 2021). The rotational profile corresponding to chromospheric temperatures (304 Å) aligns well with the findings of Mishra et al. (2024), adding credibility to our results. Additionally, our results are consistent with the Chandra et al. (2010); Morgan (2011); Sharma et al. (2020); Sharma et al. (2021); Edwards et al. (2022), suggesting that the corona rotates faster and less differentially (see Table 1).

4.2. *Variation of rotational parameters with height and temperature*

In order to investigate the variations in solar differential rotation from the photosphere to the corona, as is indicated in studies like Vats et al. (2001); Altrock (2003); Sharma et al. (2020); Imada et al. (2020), it is necessary to get the corresponding height of all AIA channels. Several 1D models of the solar atmosphere through the photosphere to the transition region have been proposed throughout the years (Vernazza et al. 1981; Fontenla et al. 1993). However, these models provide features that seldom agree with the observed profiles due to several factors (Avrett & Loeser 2008). Hence, we obtain the approximate representative heights above the photosphere to represent the parts of the solar atmosphere visible in the wavelength channels used in this study (see Table 1), keeping in mind the temperature sensitivity of the same (Simon et al. 1972, 1974; Fossum & Carlsson 2005; Kwon et al. 2010; Howe et al. 2012). Unfortunately, to the best of our knowledge, there was no singular height that could be ascribed to the AIA 131 Å Consequently, we have not included the rotation parameters measured using data from this channel in this part of the analysis. Furthermore, in order to make a fair comparison of rotational parameters across all wavelength bands, we also study the variations in rotational parameters with the temperature (T) corresponding to each wavelength.

In Figure 4, we plot the rotational parameters, A (Figure 4a) and B (Figure 4b), against the height (z) above the photosphere and T ($\log_{10} T$), whereas B with z and T in Figure 4c, Figure 4d, respectively. Finally, to assess the extent of the relationship between the said parameters, we calculated both Spearman (ρ_s) and Pearson (ρ) correlation coefficients (CC) between rotational parameters and the $\log_{10} T$. These positive values of CC, between (A, z) and (B, z), are indicative of an increase in equatorial rotation as well as the decrease in latitudinal gradient (flatter profile) with height in the solar atmosphere, which has been previously speculated by Parker et al. (1982); Japaridze et al. (1992); Wang et al. (1988); Vats et al. (2001); Altrock (2003); Sharma et al. (2020). Additionally, the relationship between A and $\log_{10} T$ seems to exhibit similar behaviour, although with lower CC. Here we would like to emphasize the scarcity of data in the temperature range from approximately $\log_{10} T = 5.0$ (represented by 1600 Å) till $\log_{10} T \approx 5.9$ (represented by 171 Å). This absence of information could potentially have a significant impact on the determination of the correlation in the present scenario. Conversely, the B shows an upward trend in connection with $\log_{10} T$. Based on Figure 4, we note that although the rotation parameters show positive CC, the nature of the increase is different in these two cases (temperature and height).

4.3. *Is there a connection with the solar interior?*

It is imperative to acknowledge from Figure 3 that the rotation rate of the solar atmosphere (for all AIA channels) is faster than that of the rotation rate measured using photospheric magnetic features like sunspots. Interestingly, the rotation rate derived using magnetic features, which are believed to be anchored deeper in the photospheric surface, is greater than the rotation rate obtained based on Doppler measurement, which samples the higher photospheric plasma (Komm et al. 1993b,a; Xiang et al. 2014; Xu & Gao 2016). Such results motivate us to consider the potential connection between the faster-rotating solar interior to the faster-rotating solar atmosphere measured in this study. In order to explore such possibilities, we need to obtain the profile of the Sun's rotation from the subsurface regime to its outer layers, observing how rotational characteristics evolve from the interior to the atmosphere of the Sun.

We have already obtained the rotation rate of the solar atmosphere whereas for internal rotation, we use the helioseismic measurement of solar rotation, obtained using the methodology outlined in Antia et al. (1998, 2008). The helioseismic data we use is the temporally averaged values of $\Omega(r, \theta)$ for $r \in [0.7\,\mathrm{R}_\odot, 1.0\,\mathrm{R}_\odot]$ in steps of $0.005\,\mathrm{R}_\odot$ and $\theta \in [0° - 88°]$ in steps of $2°$. To obtain the rotation parameters i.e., A, B and C for a given depth
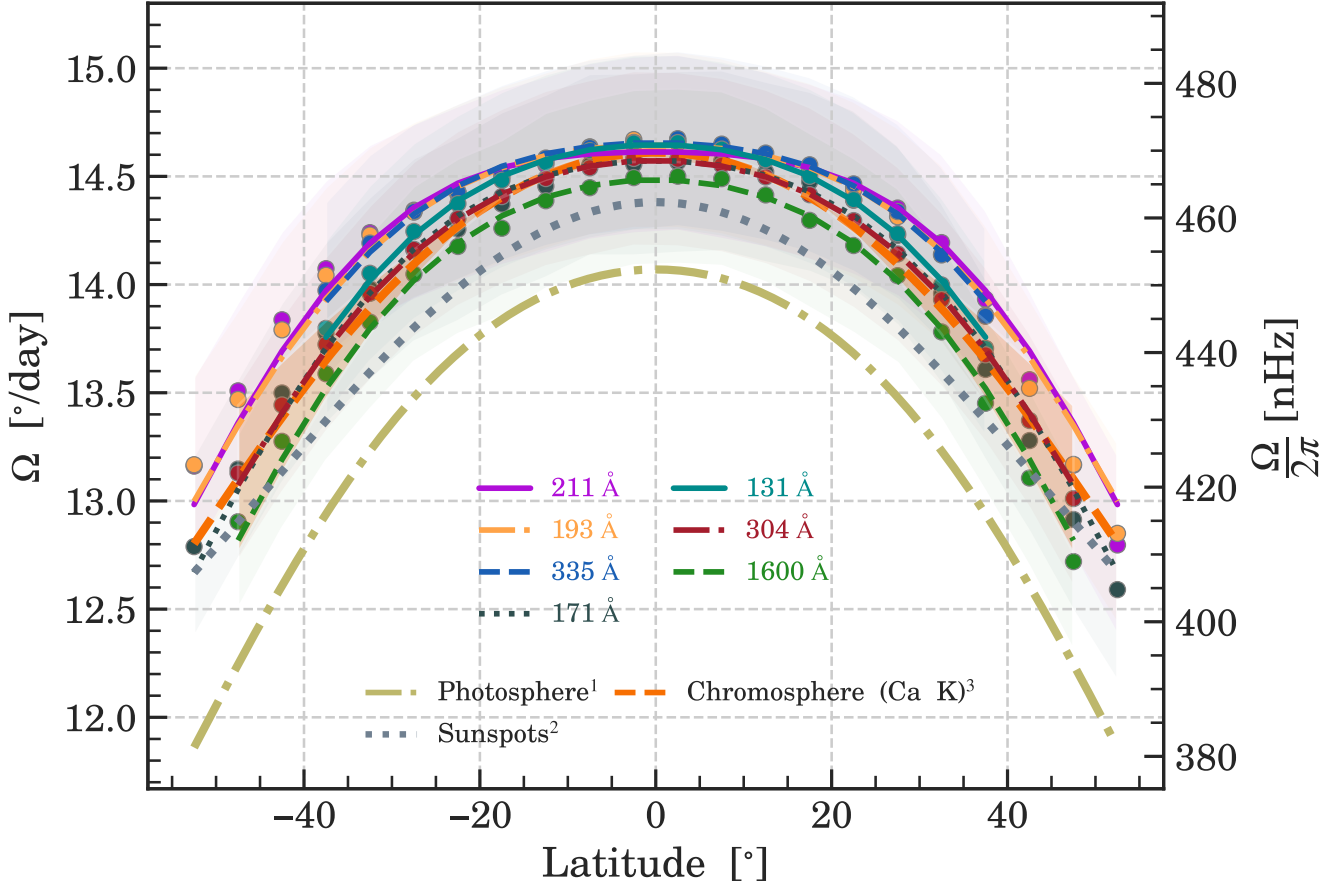
Figure 3. The average rotational profiles of all AIA channels starting from the chromosphere to corona, along with the results from [1]Snodgrass (1984), [2]Jha et al. (2021) and [3]Mishra et al. (2024).

Table 1. The values of differential rotation parameters for different wavelength channels

Wavelength (Primary ion)	$\mathrm{Log_{10}}\,T^*$	Height $\pm$ error*	$A \pm \Delta A$	$B \pm \Delta B$	$C \pm \Delta C$
(Å)		(z, km)	(°/day)	(°/day)	(°/day)
304 (He II)	4.7	2820 ± 400	14.574 ± 0.012	-1.518 ± 0.12	-2.287 ± 0.223
1600 (C IV)	5.0	430 ± 185	14.485 ± 0.024	-1.612 ± 0.243	-2.677 ± 0.452
131 (Fe VIII)	5.6	—	14.649 ± 0.014	-1.334 ± 0.200	-2.999 ± 0.519
171 (Fe IX)	5.93	5100 ± 1900	14.574 ± 0.032	-1.356 ± 0.286	-2.654 ± 0.461
193 (Fe XII)	6.176	6700 ± 2000	14.645 ± 0.039	-0.916 ± 0.344	-2.701 ± 0.557
211 (Fe XIV)	6.272	6100 ± 1900	14.613 ± 0.042	-0.504 ± 0.372	-3.314 ± 0.601
335 (Fe XVI)	6.393	15200 ± 2300	14.656 ± 0.015	-0.958 ± 0.224	-2.750 ± 0.604

NOTE—*The logarithmic temperatures and heights used to represent all wavelength channels are obtained from the studies of Simon et al. (1972, 1974); Fossum & Carlsson (2005); Kwon et al. (2010); Howe et al. (2012); Lemen et al. (2012); Nuevo et al. (2015). A detailed discussion is available in Appendix B.
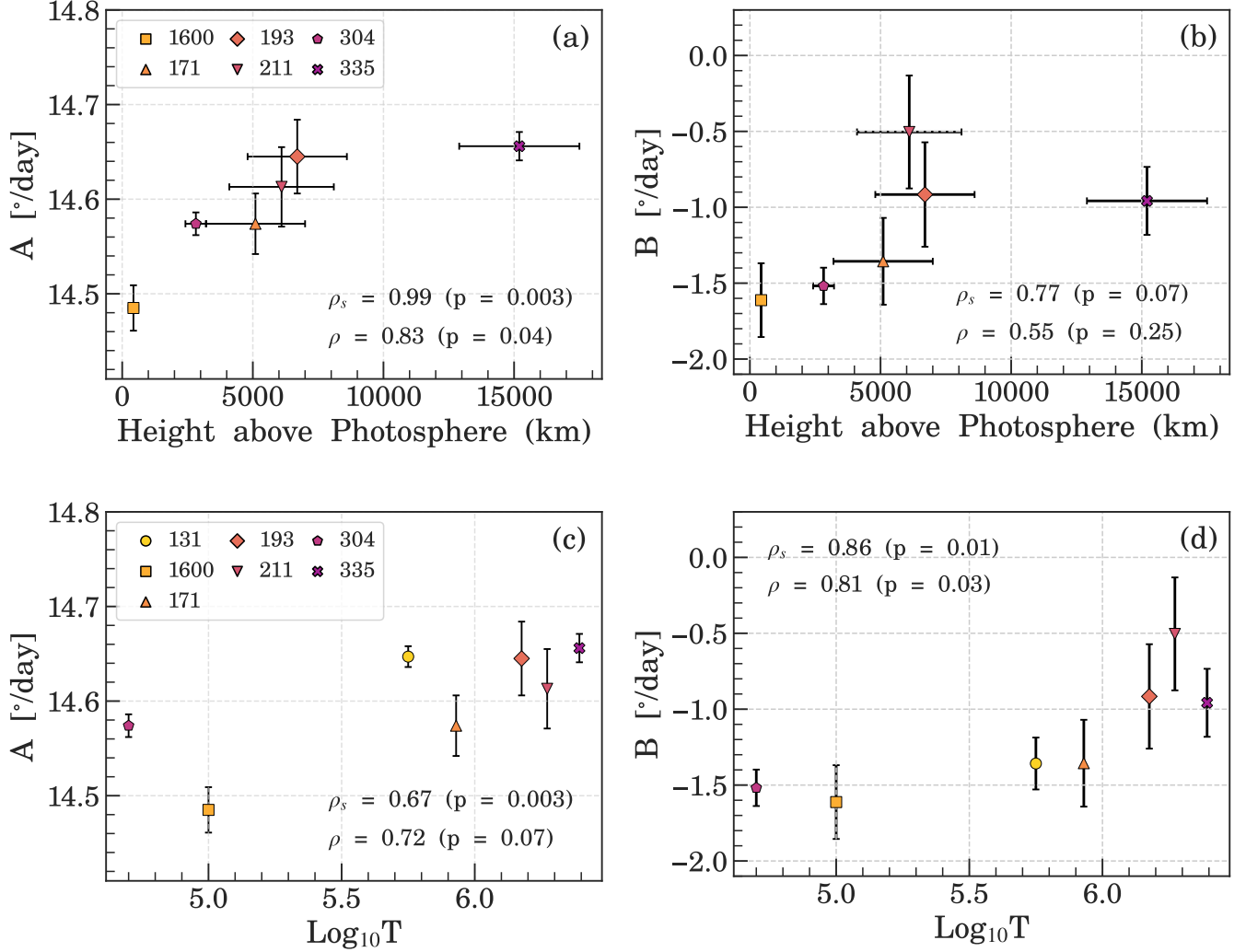
Figure 4. The trend in (a) equatorial rotation rate (A), and (b) differential gradient (B) with increasing height above the photosphere. All error bars in the $y-$axes correspond to the uncertainty pertained in determining the parameters A and B, whereas the errorbars along the $x-$axis correspond to the errors as determined by the original studies as listed in Table 1. The variation in (c) Equatorial rotation rates (d) Differential gradients of the solar atmosphere as obtained with temperature.

r we fit $\Omega(r, \theta)$ with Equation 1 for latitudes spanning $\pm 60°$ (as most of the solar magnetic features considered in this study are limited within this latitude). This calculation is only performed for all $r \in (0.93, 1.0)\,\mathrm{R}_\odot$, as we are assuming the possibility of sub-photospheric influence on solar atmospheric rotation. A representative example of rotation profile for $r = 0.94\,\mathrm{R}_\odot$ (deeper) and $r = 0.965\,\mathrm{R}_\odot$ (near the surface) is shown in Figure 5.
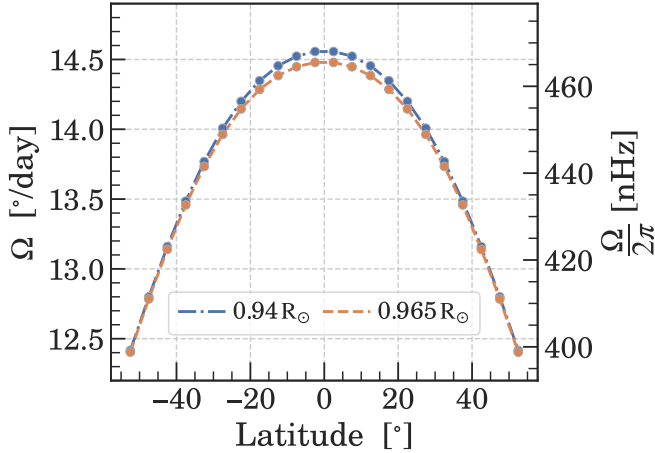
Figure 5. A representative plot of the rotational profiles obtained from helioseismological data assuming a symmetric distribution of rotation rates in both hemispheres.

To examine the evolution in rotational parameters from sub-photspheric regime to the atmospheric values obtained in this study, we compare our results with the rotation rate inferred from helioseismology with respect to depth as well as the corresponding temperature (see Figure 6), derived from Solar S-Model (Christensen-Dalsgaard et al. 1996). On comparing our results in Figure 6a, interestingly, we note that the rotation parameter A for solar atmosphere as obtained from the 304 Å and 171 Å coincide with the rotation parameter A obtained at a depth of $r \approx 0.94\,\mathrm{R}_\odot$ as well as the A for 1600 Å coincides with the A for $r \approx 0.965\,\mathrm{R}_\odot$. Additionally, we also note that the A at $r = 0.94\,\mathrm{R}_\odot$ also show a good match with the A obtained in the case of 211 Å, if we consider 3σ uncertainty for A. At this juncture, it is imperative to emphasize that the 211 Å channel receives a contribution from cooler components too, with the temperature near to the one the 171 Å channel is sensitive to. This further highlights the complexity of considering the solar atmosphere to be distinctly stratified, with the contribution from each layer being unique and independent. We acknowledge the importance of considering the potential contributions from different heights in the same channel when determining

equatorial rotation rates, as demonstrated by the case of 211 Å.

Considering the complexity associated with the determination of unique height, in Figure 6c-d, we plot A and B obtained for atmosphere as well as interior as a function of T ($\log_{10} T$) instead of the z. Interestingly, we find the exact same match with the internal rotation for these wavelengths. However, for B we do not find any such clear connection between the interior and atmosphere of the Sun (see Figure 6b and d). On plotting the respective rotational profiles for the depths of $0.94\,\mathrm{R}_\odot$ and $0.965\,\mathrm{R}_\odot$ and channels 171 Å, 304 Å and 1600 Å, we find a good overlap of the profiles for $0.965\,\mathrm{R}_\odot$ and 1600 Å at all latitudes, while for $0.94\,\mathrm{R}_\odot$, 171 Å, 304 Å, the overlap is more apparent at the equatorial regime (see Figure 7).

Such an overlap in equatorial rotation rates had also been previously discussed in Badalyan & Sýkora (2005); Mancuso et al. (2020), who had used Coronal Green Line Brightness (CGLB) data and ultraviolet (UV) spectral line observations, respectively, to obtain the rotational profile of the solar corona. Furthermore, **Ruždjak et al. (2004)** had also previously suggested the anchoring of sunspots at $0.93\,\mathrm{R}_\odot$ on a similar comparison with helioseismology results.

4.4. *Variation of rotational parameters with solar activity*

Another topic that has persistently generated significant interest and debate is the impact of solar activity on the rotation rate of the Sun. Although the limited data span makes such a study challenging, we explore whether the rotational parameters of the solar atmosphere vary with solar activity, i.e., with the different phases of the solar cycle. To achieve this, we obtained the differential rotation parameters (A, B and C) for each year using a similar approach as discussed in Section 4. These parameters are then plotted in Figure 8 as a function of time along with the yearly averaged sunspot number (SSN)[4], which is a marker for solar activity.

In Figure 8, we note an apparent cyclic behaviour with time in the rotational parameters, both A and B. To quantify this behaviour, we calculate the Spearman rank correlation (ρ_s) of the parameters obtained for each channel with the SSN (see Table 2). We note that the results from the channel 1600 Å as well as the channels with sensitivity to temperatures native to coronal heights (171 Å, 193 Å, 211 Å, 131 Å and 335 Å) show
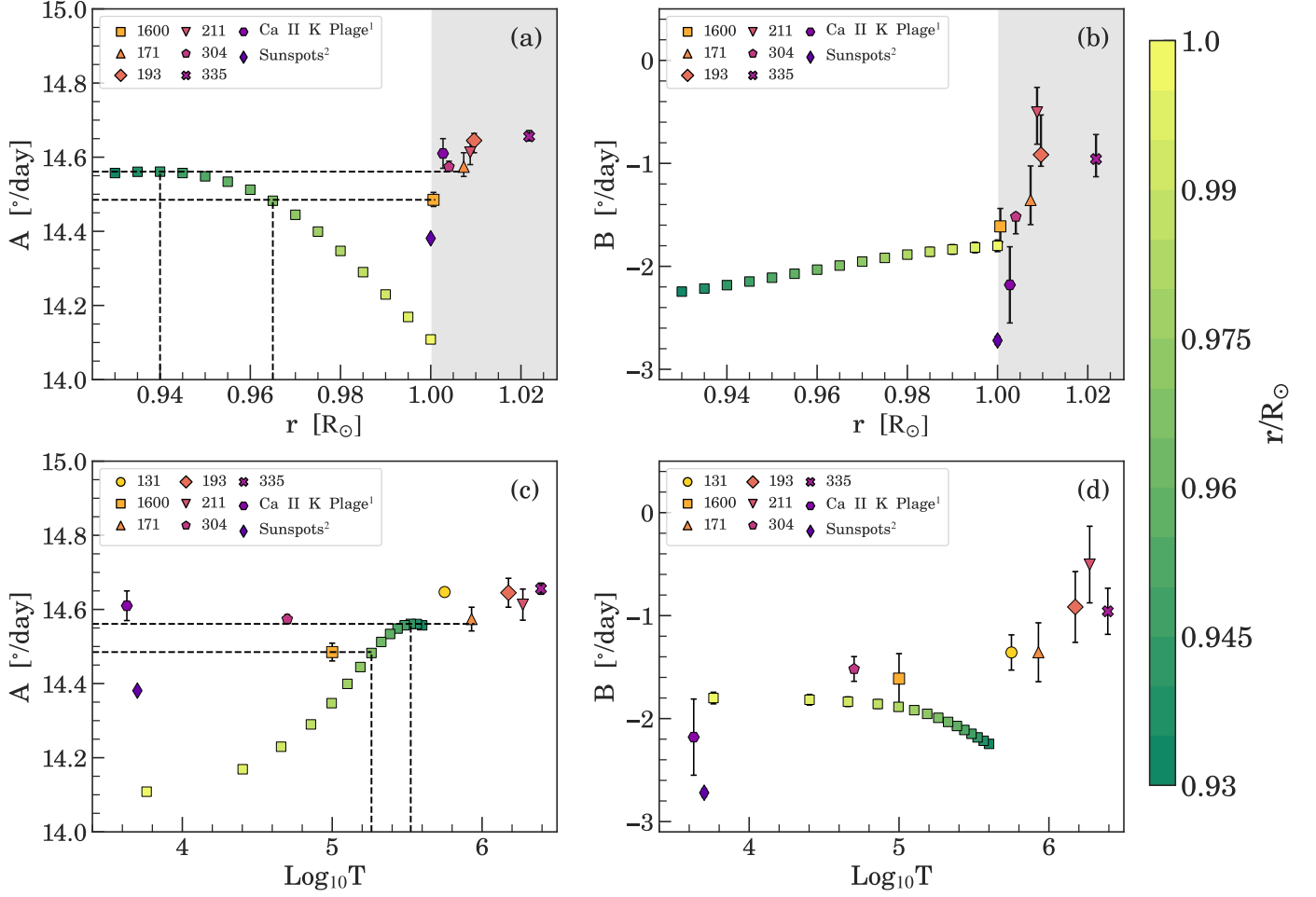
---

[4] https://www.sidc.be/SILSO/datafiles

Figure 6. The variation in rotational parameters Equatorial Rotation rate (A) and Latitudinal gradient (B) from the interior to the atmosphere (highlighted in grey) of the Sun as a function of radius (top panel; (a) and (b)) and logarithmic temperature (bottom panel; (c) and (d)), as obtained from this study, [1]Mishra et al. (2024), [2] Jha et al. (2021) and helioseismology. The height representative of Ca II K plages is obtained from Stix (1976) while the logarithmic temperature is obtained from Beebe (1971)
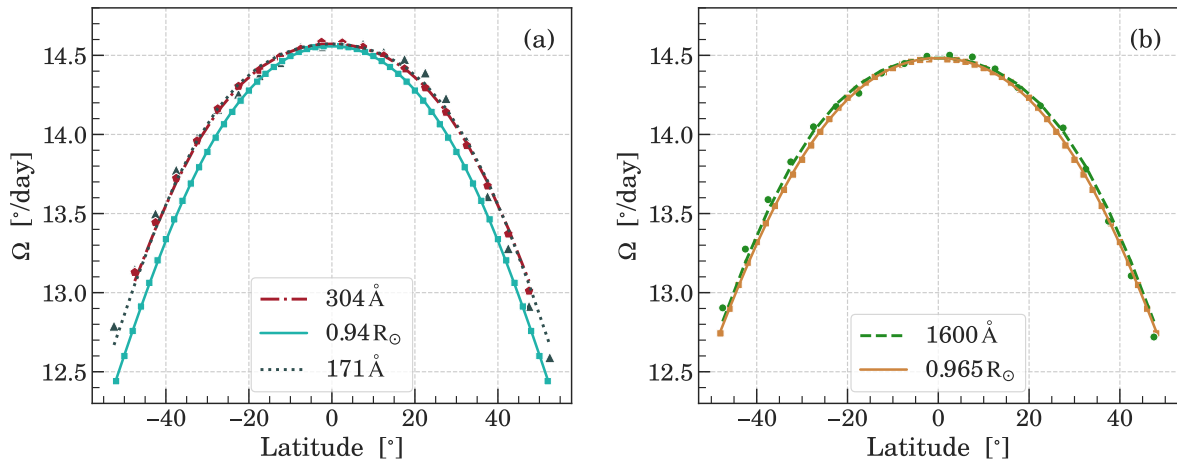
Figure 7. Comparison of the rotational profile at the depth of (a) $0.94\,R_\odot$, with that obtained for 171 Å and 304 Å; and (b) 1600 Å with $0.965\,R_\odot$ at all latitudes.

a significant positive correlation in equatorial rotation   rate, A, with solar cycle phase (p< 0.05). Such a corre-
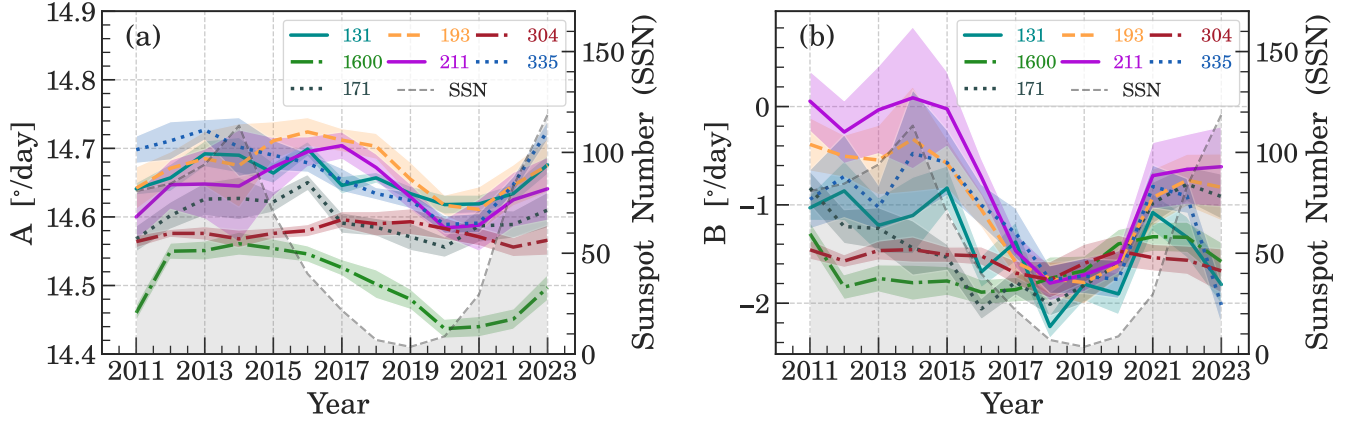
Figure 8. The variation in rotational constants with the progression of cycles 24 and 25 compared with the sunspot number. The shaded area in each colour represents the uncertainty in determining the respective parameters.

lation of the differential rotation of different parts of the solar corona with the solar activity cycle has been reported in many studies (Vats et al. 1998; Li et al. 2012; Javaraiah 2013; Jurdana-Šepić et al. 2011; Xie et al. 2017; Imada et al. 2020). In contrast, the chromospheric channel (304 Å) shows a very low and negative value of CC, thereby barely indicating any variation with solar activity. This behaviour of the chromospheric rotational profile is consistent with the results for chromospheric rotation as obtained in Mishra et al. (2024) and Jha et al. (2021) for sunspot, who found no significant change in equatorial rotation rate with solar activity. However, on studying cyclic variation of differential rotation parameters using sunspot data from various databases, Ruždjak et al. (2017) found that the equatorial rotation rate does reach its maximum just before solar activity minimum, which can be noticed from a careful comparison of the general trend of A with solar activity.

For parameter B, which represents the differential nature of the rotation, we find no such significantly high positive correlation ($p < 0.05$) in any channel other than 211 Å. Jurdana-Šepić et al. (2011) obtained a similar lack of correlation for parameter B; however, they attributed this lack of correlation to more pronounced errors in their data at higher latitudes.

5. DISCUSSION

The rotational profiles of the upper solar atmosphere in Figure 3, as seen in different wavelength regimes, suggest that the solar atmosphere, as modulated by magnetic large-scale features like plages, CBPs, filaments, coronal loops, etc., rotates $2.95\% - 4.18\%$ and $0.73\% - 1.92\%$ faster (at the equator) and less differentially compared to the photospheric rotational profile obtained from dopplergrams and sunspot data, respectively. However, these results are obtained based on

Table 2. Spearman rank correlation coefficients of the rotational parameters and yearly averaged Sunspot numbers (SSN).

Wavelengths	A		B	
(Å)	ρ_s	p-value	ρ_s	p-value
304	-0.309	0.304	0.269	0.374
1600	0.863	0.001	-0.52	0.069
131	0.813	0.001	0.489	0.09
171	0.863	0.001	0.148	0.629
193	0.583	0.036	0.67	0.012
211	0.571	0.041	0.725	0.005
335	0.83	0.0005	0.462	0.112

the method of image correlation, which is sensitive to the intensity contrast of multiple magnetic features in the hotter solar atmosphere. While this method does not distinguish between the rotation of individual features, this method has the advantage of improving the statistics of the analysis by taking into account all the features distinguishable by intensity. The hotter solar atmosphere is also an optically thin region, and therefore, a measurement of shift in features could also be affected by the line-of-sight effect, leading to an apparent measurement of faster rotation. Therefore, there is a possibility that these results have an effect of the apparent line-of-sight (LoS) effect arising because of the extended structures like coronal loops. To test this hypothesis, we created a toy model of an extended structure mimicking a coronal loop to examine the extent of such an effect (see Appendix A). The results obtained based on this experiment have confirmed that the difference between the photospheric rotation rates and that beyond the photosphere can not only be the outcome of

the line-of-sight effect. However, it might have a small effect on it, which we have quantified in Appendix A.

Once we have eliminated this prospect, it is important to acknowledge that the solar atmosphere is not uniformly stratified and is multi-thermal; consequently, a filter sensitive to a specific temperature may receive contributions from various heights. However, this study relies on the well-established understanding that certain global temperature ranges (e.g., $\approx 10^6$ K) are limited to the higher layers of the solar atmosphere (e.g., the solar corona). Although these temperatures may be instantaneously achieved locally in the lower layers of the solar atmosphere during transient events (e.g., flares), we assume they do not represent the long-term global characteristics of the solar atmosphere, which is the primary focus of this study. As a result, the outcomes derived in this study remain statistically unaffected by these events.

The observed increasing trend in the solar differential rotation with height is a very debatable topic, and the proper explanation for such behaviour is still incomplete. However, a theoretical perspective was proposed by Weber (1969), discussing the role of magnetic field line configuration on atmospheric rotation leading to an increasing rotation rate with height which is in agreement with our measurement. According to Weber (1969), the interplay between magnetic field torque and the velocity plasma flowing outward ensures that the rotation rate increases with an increase in radial distance to keep the total angular momentum conserved. Additionally, the role of the magnetic field in providing the angular momentum required for faster rotation of the solar atmosphere beyond the photosphere has also been suggested in many studies (Komm et al. 1993b; Badalyan & Sýkora 2005; Kwon et al. 2010; Badalyan 2010; Badalyan & Obridko 2018; Li et al. 2019; Imada et al. 2020; Edwards et al. 2022)

In Section 4.3, we find an excellent match between the equatorial rotational (A) rate at the depths of $r = 0.94\,\mathrm{R}_\odot$ and $r = 0.965\,\mathrm{R}_\odot$ as inferred in helioseismic observations, with that obtained for the channels 304 Å, 171 Å and 1600 Å. While this alignment may seem coincidental, the potential physical connection between them cannot be completely dismissed owing to Ferraro's law of isorotation (Ferraro 1937), which hints toward such a possibility. According to this law, strong magnetic fields frozen in plasma tend to transport the angular momentum at their footpoints throughout their extent; thereby leading to a comparatively rigid nature of rotation in low β plasma and we suspect that this could be the region behind the observed behaviour of solar rotation. The idea that the footpoints of the loops

visible in 171 Å may have their root in the lower layers has been also suggested in works like that of Kwon et al. (2010), while several works have also hinted at the possibility of sub-photospheric rooting of coronal magnetic features (Zaatri et al. 2009; Bagashvili et al. 2017; Edwards et al. 2022; Kutsenko et al. 2022). We emphasize here that, these arguments should be taken with a grain of salt and it needs a better and thorough study to confirm such possibility.

We have also observed a positive correlation between the changes in the rotation of the solar atmosphere and the phase of the solar cycle, as evidenced by the correlation with the yearly averaged sunspot number, more prominent in the rotational parameter A. Such a result could indicate a relationship between the solar atmospheric rotation and the presence of different magnetic structures (e.g., plages, coronal loops, CBPs etc.) during different phases of solar activity. Another possibility hints at the probable existence of a phenomenon called torsional oscillation, which has extensively been discussed and documented in various studies (e.g., Komm et al. 1993a; Imada et al. 2020). Notably, the possibility of such a phenomenon is prominently observed in the layers at coronal temperatures (171 Å, 193 Å, 131 Å, 211 Å), while no such variation is observed in the chromospheric counterpart (304 Å) in agreement with the findings of Mishra et al. (2024) for the chromosphere and (Jha et al. 2021) for sunspots. Additionally, the variation of the coronal rotational profile has been proposed to be affected by magnetic flux concentrations (Komm et al. 1993a; Weber et al. 1999; Altrock 2003; Imada et al. 2020), which is positively correlated with solar activity.

Additionally from Figure 8, it is also apparent that the parameter A reaches its maximum just before the minimum, while the parameter $|B|$ has a greater value at cycle minimum for 211 Å, suggesting a more differential rotation at cycle minimum. This is similar to the results obtained by Ruždjak et al. (2017) and can be suggestive of what is known as the braking effect exerted by non-axisymmetric magnetic fields (Brun 2004). Theoretical efforts have been made to explain such a variation with cycle activity, results from which have highlighted the role of the strength of magnetic fields in the transport of angular momentum towards the equator (Brun 2004; Brun et al. 2004; Lanza 2006, 2007; Brun & Rempel 2009).

Except 211 Å, no statistically significant correlation of the parameter B with the yearly averaged sunspot number is apparent for most pass bands representing the hotter solar atmosphere. A possible connection can be made to the cross-talk between the parameters B and

C, which amplifies the noise-related uncertainties and obscures their actual time variation (Snodgrass 1984). This cross-talk is also the reason why the individual variation in the parameter C is not individually examined in the study.

6. SUMMARY & CONCLUSION

In this study, we analyzed 13 years of SDO/AIA data to understand the solar atmospheric rotational profile, its variation at different layers of the solar atmosphere, and with parameters like temperature and solar activity. The primary conclusion we arrive at in this study is that the solar atmosphere, till lower coronal heights, rotates faster and less differentially compared to the photospheric rotation rates obtained from Dopplergrams and sunspot data.

The study also utilised data from helioseismology at different depths to understand the variation of the rotational profile from the interior to the atmosphere and subsequently found a significant correlation between the rotational rate at certain sub-photospheric depths $(0.94\,R_\odot, 0.965\,R_\odot)$ and that obtained for the channels sensitive to certain temperatures of the solar atmosphere $(171\,\text{Å}, 304\,\text{Å}$ and $1600\,\text{Å}$ respectively).

While the current study has reinforced that the hotter solar atmosphere indeed does rotate faster and less differentially than the photosphere, numerous unanswered questions remain. Despite the few possibilities explored in this study, the physical understanding behind the observed increase in rotation rate and decrease in differential nature and their generalized trends with height above the photosphere, logarithmic temperature, and solar activity remains unclear. It is important to note that this study does not aim to provide detailed information about the rotational profiles at each specific temperature and height within each layer of the solar atmosphere but rather to provide an overview of the general trend in the rotation of the solar atmosphere from the photosphere to the chromosphere, transition region, and corona.

The findings of this study, if revisited with a larger dataset encompassing multiple cycles and a method capable of distinguishing between thermally distinct features at their exact height of formation, might have significant implications in our understanding of the overall behaviour of the Sun's differential rotation and its complex relationship with the solar magnetic field. A future study could focus on developing a method to isolate the high- and low-temperature components in images from each channel as well as isolating the specific height associated with them to map the variation in the rotational profile of the exact same feature at different heights of the solar atmosphere, which is crucial for a more thorough analysis. Further validation for the trends suggested in this study can also be provided through the use of a dataset that spans multiple solar activity cycles as well as through the use of orthogonalized fit functions. This will help mitigate any potential biases that may have arisen from using a dataset that spans fewer cycles.

APPENDIX

A. EXPLORING THE EFFECT OF LINE OF SIGHT (LOS) PROJECTION OF EXTENDED STRUCTURES ON THE RESULT

We have shown that the solar atmosphere, modulated by structures like plages, coronal loops, active regions, filaments etc., rotates faster than the photosphere ($\Delta\Omega \in [0.105, 0.558]°$/day). The extended height of such features above the photosphere, especially at higher latitudes, can result in an erroneous measurement of the rotation rate based on projected coordinates (Roša et al. 1998; Vršnak et al. 1999; Sudar et al. 2015). Although the image correlation technique utilised in this study is tracer-independent and considers only the pixel-specific integrated intensity along the LoS to calculate the rotation rate in a particular latitudinal bin through the calculation of the 2-D cross-correlation coefficient, this method may be sensitive to the angle with respect to the LoS, and structures extending from the solar disk, such as coronal loops, whose position with respect to the LoS may influence the value of the intensity populating specific pixels and, consequently, the results obtained through image correlation. To investigate the impact of such scenarios, a simplified toy model was created, mimicking extended structures whose LoS integrated intensity changes only with respect to their position relative to the LoS, while the footpoint of the structure remains stationary. This was done to isolate the excess rotation rate resulting from the LoS effect ($\Delta\Omega_{LoS}$). The model was designed with two different spatial resolutions: (a) with a smaller pixel size corresponding to a better resolution (Golub & Kalata 1986), wherein 1 pixel corresponds to 100 km in the sky; and (b) the coarser AIA pixel size, wherein 1 pixel corresponds to 435 km in the sky (Alissandrakis 2019) (Figure 9). The aim was twofold: (i) to determine whether the LoS projection effect contributes to the disparity in rotation rate between the photosphere and the hotter solar atmosphere modulated by extended structures like coronal loops; and (ii) if it does, to assess the relevance of this effect in our study using data from SDO/AIA.

Once the projected intensity along the LoS (I_{LoS}) is obtained for a specific angle (θ), the structure is shifted by a constant angle ($\Delta\theta$), which represents the anticipated change in the angle with respect to the LoS of the structure, calculated from the rotation period of the footpoint (assuming it is the solar surface) at the equator and a cadence of 6 hours. The structure is now positioned at an angle $\theta + \Delta\theta$ relative to the LoS, and the projected intensity obtained is cross-correlated with the projected intensity obtained at the initial angle θ. The resulting shift is used to calculate the excess in rotation rate ($\Delta\Omega_{LoS}$), which is represented as the excess in rotation rate for the LoS angle θ. This process was repeated for all LoS angles in the progression of $\theta + 2\Delta\theta$, $\theta + 3\Delta\theta$, and so on, spanning $\pm45°$ in longitude. This approach was taken to match the conditions imposed on the data in the original analysis. The results obtained for a synthetic structure of length 5 Mm observed at a high resolution of 100 km/pixel suggest an excess rotation rate ($\Delta\Omega_{LoS}$) of up to $\approx 0.83°$/day (see Figure 10 (a)), which is higher than the excess obtained in our original analysis. This suggests that when data at higher resolutions is subjected to the image correlation method without any pre-processing, there might be a LoS projection effect that affects the results obtained.

To see if such an effect can affect our analysis using AIA data, which offers a much coarser resolution, we create a much larger structure (Length= 150 Mm; see Figure 9 (b)) and subject it to the same process of analysis. The results thus obtained suggest an excess of up to $\Delta\Omega_{LoS} \approx 0.002°$/day (see Figure 10 (b)), which is not enough to explain the excess rotation rate of the extended structure-modulated solar atmosphere observed in our analysis. In light of these results, we would like to emphasize that, as part of our analysis, we employed pre-processing techniques such as Gaussian smoothing (see section 3), which has a blurring effect and further degrades the resolution, thus minimizing the likelihood of spurious effects like the one discussed here. These findings provide further evidence that the faster rotation of the solar atmosphere is a complex physical phenomenon rather than a data or method-specific artefact.

B. REPRESENTATION OF HEIGHT AND LOGARITHMIC TEMPERATURE FOR AIA CHANNELS

The approximate heights used to represent the different channels of the SDO/AIA are obtained from previous studies, as discussed below,

- The heights and their respective uncertainties used to represent channels 304 Å, 1600 Å and 335 Å are the formation heights for He II, C IV and Fe XVI emission lines as obtained in Simon et al. (1972, 1974); Fossum & Carlsson (2005); Howe et al. (2012)
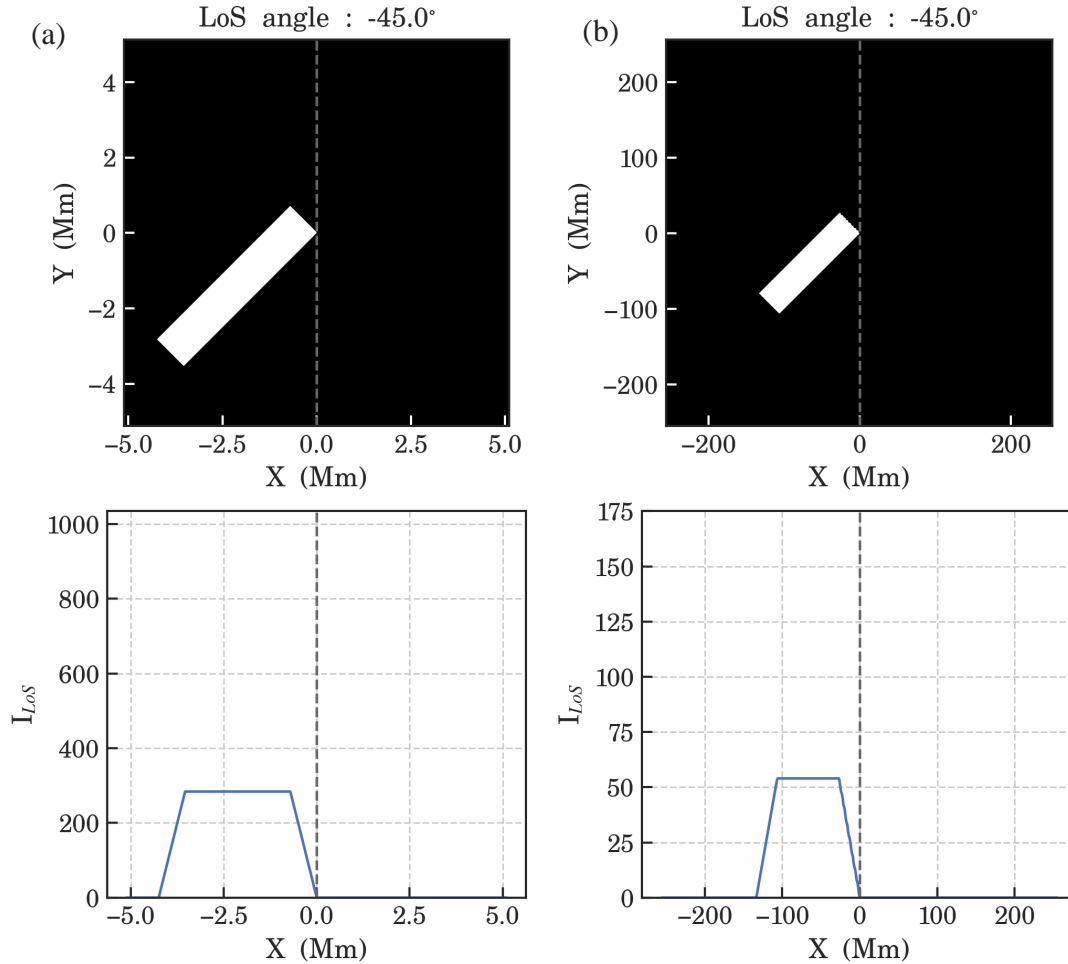
Figure 9. (Top) Still example images of a toy model simulating an extended structure similar to a coronal loop, with a static point of anchoring, such that only the object's angle with respect to the LoS (denoted by the vertical dotted line) is changing, and (bottom) the LoS integrated intensity of the same structure at (a) pixel scale of 100 km/pixel. (b) pixel scale of the SDO/AIA, i.e, 435 km/pixel. This figure is available as an animation in the online version of the article. The total duration of the animation is 8 s.

- For the channels 171 Å, 193 Å and 211 Å, we utilized the heights determined by Kwon et al. (2010) through the study of coronal bright points (CBPs) from the data of the 171 Å, 195 Å, and 284 Å channels of the Solar TErrestrial RElations Observatory (STEREO). This was done keeping in mind that the CBPs, as well, are structures which dominate in the cross-correlation process through which the rotational profile is determined for these wavelength channels of SDO/AIA. Furthermore, the logarithmic temperatures represented by the 195 Å and 284 Å channels of STEREO are nearest to the 193 Å and 211 Å channels of the AIA, respectively.

The logarithmic temperatures used to represent the wavelength channels of AIA were taken from Lemen et al. (2012); Nuevo et al. (2015) and represent the temperature responses of these respective AIA filters. Its important to point out that even though the 131 Å and 193 Å channels are also sensitive to hot flare plasma ($\mathrm{Log}_{10}\mathrm{T} = 7.0$), the nature of our study focuses only on the long-term events with lifespan > 0.25 days or 6 hours. So, we assume the cooler component of this wavelength band contributes primarily to our results (see Figure 11).

REFERENCES

Adams, W. M., & Tang, F. 1977, SoPh, 55, 499,
    doi: 10.1007/BF00152590

Alissandrakis, C. E. 2019, SoPh, 294, 161,
    doi: 10.1007/s11207-019-1552-1
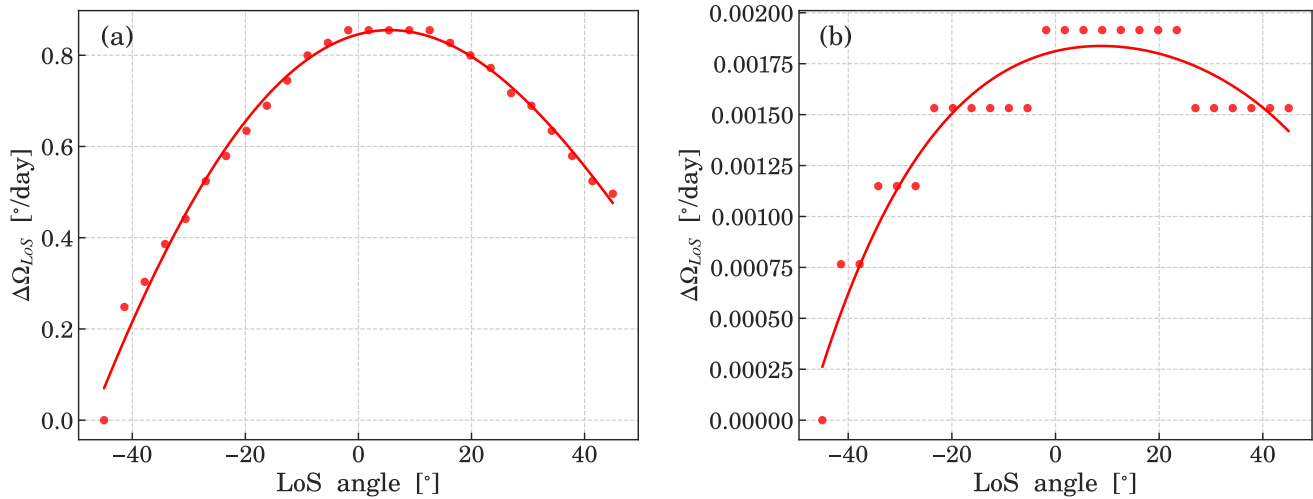
Figure 10. The variance of $\Delta\Omega_{\text{LoS}}$ for change in LoS angle for a (a) 5 Mm structure in high resolution (b) 150 Mm structure in AIA resolution. An order 4 regression fit has been used to show the general trend in $\Delta\Omega_{LoS}$
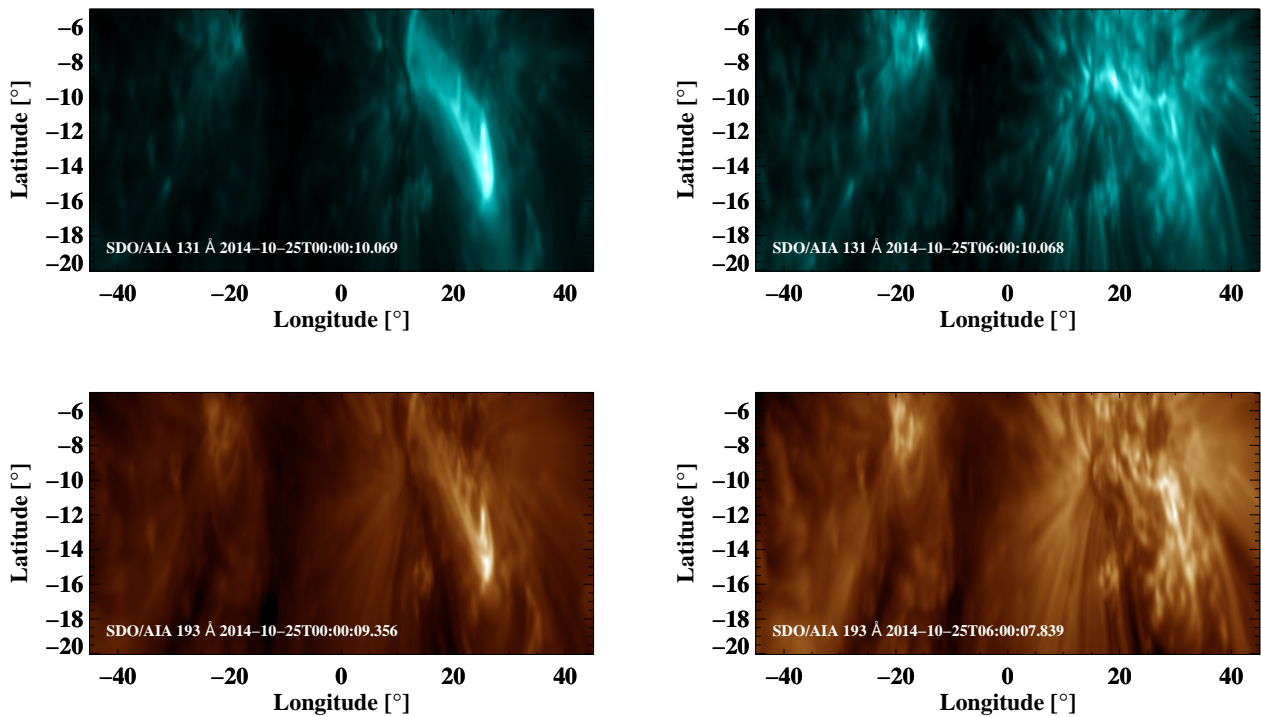
Figure 11. An example image with flare from 2014, October, 25 in heliographic coordinates after smoothing as visible in 131 Å (top) and 193 Å (bottom) channels. Since flares are spontaneous, short-term transient events with a life span much less than 6 hours, we assume they do not contribute to our long-term correlation analysis. So, the channels 131 Å and 193 Å are represented by their cooler counterparts contributed to primarily by Fe VII and Fe XII ($\text{Log}_{10}\text{T} = 5.8, 6.2$), respectively.

Altrock, R. C. 2003, Solar Physics, 213, 23,
doi: 10.1023/A:1023204814099

Antia, H. M., Basu, S., & Chitre, S. M. 1998, Monthly
Notices of the Royal Astronomical Society, 298, 543,
doi: 10.1046/j.1365-8711.1998.01635.x

—. 2008, The Astrophysical journal

Aschwanden, M. J., Boerner, P., Schrijver, C. J., &
Malanushenko, A. 2013, Solar Physics, 283, 5,
doi: 10.1007/s11207-011-9876-5

Aslanov, I. A. 1964, Soviet Ast., 7, 794

Avrett, E. H., & Loeser, R. 2008, ApJS, 175, 229,
doi: 10.1086/523671

Badalyan, O. G. 2010, New Astronomy, 15, 135,
doi: 10.1016/J.NEWAST.2009.04.006

Badalyan, O. G., & Obridko, V. N. 2018, Astronomy
Letters 2018 44:11, 44, 727,
doi: 10.1134/S1063773718110014

Badalyan, O. G., & Sýkora, J. 2005, Contributions of the
Astronomical Observatory Skalnate Pleso, 35, 180

Bagashvili, S. R., Shergelashvili, B. M., Japaridze, D. R.,
et al. 2017, Astronomy and Astrophysics, 603,
doi: 10.1051/0004-6361/201630377

Balthasar, H., Vazquez, M., & Woehl, H. 1986, A&A, 155,
87

Beebe, H. A. 1971, Solar Physics, 17, 304,
doi: 10.1007/BF00150034

Bertello, L., Pevtsov, A. A., & Ulrich, R. K. 2020, ApJ,
897, 181, doi: 10.3847/1538-4357/ab9746

Bhatnagar, A., & Livingston, W. 2005, Fundamentals of
Solar Astronomy (WORLD SCIENTIFIC),
doi: 10.1142/5171

Bhatt, H., Trivedi, R., Sharma, S. K., & Vats, H. O. 2017,
Solar Physics, 292, 1,
doi: 10.1007/S11207-017-1071-X/FIGURES/4

Brajša, R., Vršnak, B., Ruždjak, V., et al. 1991, SoPh, 133,
195, doi: 10.1007/BF00149885

Brajša, R., Wöhl, H., Vršnak, B., et al. 2004, Astronomy
and Astrophysics, 414, 707,
doi: 10.1051/0004-6361:20034082

Brajša, R., Ruždjak, V., Vršnak, B., et al. 1999, SoPh, 184,
281, doi: 10.1023/A:1005124022163

Brun, A. S. 2004, SoPh, 220, 333,
doi: 10.1023/B:SOLA.0000031384.75850.68

Brun, A. S., Miesch, M. S., & Toomre, J. 2004, ApJ, 614,
1073, doi: 10.1086/423835

Brun, A. S., & Rempel, M. 2009, SSRv, 144, 151,
doi: 10.1007/s11214-008-9454-9

Carrington, R. C. 1859, MNRAS, 19, 81,
doi: 10.1093/mnras/19.3.81

Chamberlin, P., Pesnell, W. D., & Thompson, B. 2012, The
Solar Dynamics Observatory,
doi: 10.1007/978-1-4614-3673-7

Chandra, S., Vats, H. O., & Iyer, K. N. 2010, Monthly
Notices of the Royal Astronomical Society, 407, 1108,
doi: 10.1111/J.1365-2966.2010.16947.X

Charbonneau, P. 2010, Liv. Rev. Sol. Phys., 7, 3,
doi: 10.12942/lrsp-2010-3

Christensen-Dalsgaard, J., Dappen, W., Ajukov, S. V.,
et al. 1996, Science, 272, 1286,
doi: 10.1126/science.272.5266.1286

Chung, M. K. 2012, arXiv e-prints, arXiv:2007.09539,
doi: 10.48550/arXiv.2007.09539

Deforest, C. E. 2004, Solar Physics, 219, 3,
doi: 10.1023/B:SOLA.0000021743.24248.b0

Edwards, L. T., Kuridze, D., Williams, T., & Morgan, H.
2022, The Astrophysical Journal, 928, 42,
doi: 10.3847/1538-4357/ac54ba

Evershed, J. 1925, MNRAS, 85, 607,
doi: 10.1093/mnras/85.7.607

Ferraro, V. C. A. 1937, Monthly Notices of the Royal
Astronomical Society, 97, 458,
doi: 10.1093/mnras/97.6.458

Finley, A. J., & Brun, A. S. 2023, A&A, 679, A29,
doi: 10.1051/0004-6361/202347445

Fisher, R., & Sime, D. G. 1984, ApJ, 287, 959,
doi: 10.1086/162753

Fontenla, J. M., Avrett, E. H., & Loeser, R. 1993, ApJ,
406, 319, doi: 10.1086/172443

Fossum, A., & Carlsson, M. 2005, The Astrophysical
Journal, 625, 556, doi: 10.1086/429614

Freeland, S. L., & Handy, B. N. 1998, SoPh, 182, 497,
doi: 10.1023/A:1005038224881

Gary, G. A. 2001, SoPh, 203, 71,
doi: 10.1023/A:1012722021820

Glackin, D. L., Glackin, & L., D. 1974, SoPh, 36, 51,
doi: 10.1007/BF00151542

Golub, L., & Kalata, K. 1986, 0733, doi: 10.1117/12.964957

Gupta, S. S., Sivaraman, K. R., & Howard, R. F. 1999,
SoPh, 188, 225, doi: 10.1023/A:1005229124554

Hale, G. E. 1908, ApJ, 27, 219, doi: 10.1086/141548

Hansen, R. T., Hansen, S. F., & Loomis, H. G. 1969, SoPh,
10, 135, doi: 10.1007/BF00146162

Hapgood, M. A., Dimbylow, T. G., Sutcliffe, D. C., et al.
1997, SSRv, 79, 487, doi: 10.1023/A:1004954504114

Howard, R., Gilman, P. I., & Gilman, P. A. 1984, ApJ, 283,
373, doi: 10.1086/162315

Howard, R., & Harvey, J. 1970, Solar Physics 1970 12:1, 12,
23, doi: 10.1007/BF02276562

Howe, R. 2009, SoPh, 6, 1,
doi: https://doi.org/10.12942/lrsp-2009-1

Howe, R., Jain, K., Bogart, R. S., Haber, D. A., & Baldner,
C. S. 2012, SoPh, 281, 533,
doi: 10.1007/s11207-012-0097-3

Imada, S., Matoba, K., Fujiyama, M., & Iijima, H. 2020,
Earth, Planets and Space, 72, 1,
doi: 10.1186/S40623-020-01314-Y

Japaridze, D. R., Gigolashvili, M. S., Japaridze, D. R., &
Gigolashvili, M. S. 1992, SoPh, 141, 267,
doi: 10.1007/BF00155179

Javaraiah, J. 2013, SoPh, 287, 197,
doi: 10.1007/s11207-013-0345-1

Javaraiah, J., Bertello, L., & Ulrich, R. K. 2005, SoPh, 232,
25, doi: 10.1007/s11207-005-8776-y

Jha, B. K. 2022, PhD thesis, Pondicherry University,
doi: 10.5281/zenodo.7651499

Jha, B. K., Priyadarshi, A., Mandal, S., Chatterjee, S., &
Banerjee, D. 2021, SoPh, 296, 25,
doi: 10.1007/s11207-021-01767-8

Jurdana-Šepić, R., Brajša, R., Wöhl, H., et al. 2011, A&A,
534, A17, doi: 10.1051/0004-6361/201014357

Komm, R., Howe, R., Hill, F., & Hernández, I. G. 2008,
Solar Physics 2008 254:1, 254, 1,
doi: 10.1007/S11207-008-9285-6

Komm, R. W., Howard, R. F., & Harvey, J. W. 1993a,
SoPh, 143, 19, doi: 10.1007/BF00619094

—. 1993b, SoPh, 145, 1, doi: 10.1007/BF00627979

Kutsenko, A. S., Abramenko, V. I., & Litvishko, D. V. 2022

Kwon, R.-Y., Chae, J., & Zhang, J. 2010, The Astrophysical
Journal, 714, 130, doi: 10.1088/0004-637X/714/1/130

Lanza, A. F. 2006, MNRAS, 373, 819,
doi: 10.1111/j.1365-2966.2006.11085.x

—. 2007, A&A, 471, 1011, doi: 10.1051/0004-6361:20077418

Lemen, J. R., Title, A. M., Akin, D. J., et al. 2012, Solar
Physics, 275, 17, doi: 10.1007/S11207-011-9776-8

Lewis, D. J., Simnett, G. M., Brueckner, G. E., et al. 1999

Li, K., Shi, X. J., Xie, J., et al. 2013, Monthly Notices of
the Royal Astronomical Society, 433, 521,
doi: 10.1093/mnras/stt744

Li, K., Xu, J., Yin, Z., & Feng, W. 2019, The Astrophysical
Journal, 875, 90, doi: 10.3847/1538-4357/ab0f3a

Li, K. J., Shi, X. J., Feng, W., et al. 2012, MNRAS, 423,
3584, doi: 10.1111/j.1365-2966.2012.21155.x

Livingston, W. C. 1969, Solar Physics, 9, 448,
doi: 10.1007/BF02391670

Mancuso, S., Giordano, S., Barghini, D., & Telloni, D.
2020, A&A, 644, doi: 10.1051/0004-6361/202039094

Meunier, P., & Leweke, T. 2003, Experiments in Fluids, 35,
408, doi: 10.1007/s00348-003-0673-2

Mishra, D. K., Routh, S., Jha, B. K., et al. 2024, The
Astrophysical Journal, 961, 40,
doi: 10.3847/1538-4357/ad1188

Morgan, H. 2011, The Astrophysical Journal, 738, 189,
doi: 10.1088/0004-637X/738/2/189

Newton, H. W., & Nunn, M. L. 1951, Monthly Notices of
the Royal Astronomical Society, 111, 413,
doi: 10.1093/mnras/111.4.413

Nuevo, F. A., Vásquez, A. M., Landi, E., & Frazin, R.
2015, ApJ, 811, 128, doi: 10.1088/0004-637X/811/2/128

Parker, E. N. 1955a, ApJ, 122, 293, doi: 10.1086/146087

—. 1955b, ApJ, 121, 491, doi: 10.1086/146010

Parker, G. D., Hansen, R. T., & Hansen, S. F. 1982, Solar
Physics, 80, 185, doi: 10.1007/BF00153432/METRICS

Pesnell, W. D., Thompson, B. J., & Chamberlin, P. C.
2012, The Solar Dynamics Observatory (SDO), ed.
P. Chamberlin, W. D. Pesnell, & B. Thompson (New
York, NY: Springer US), 3–15,
doi: 10.1007/978-1-4614-3673-7_2

Pneuman, G. W., Pneuman, & W., G. 1971, SoPh, 19, 16,
doi: 10.1007/BF00148819

Pozuelo, S., Asensio Ramos, A., de la Cruz Rodríguez, J.,
Trujillo Bueno, J., & Martínez González, M. J. 2023,
arXiv e-prints, arXiv:2302.04258,
doi: 10.48550/arXiv.2302.04258

Riha, L., Fischer, J., Smid, R., & Docekal, A. 2007, in 2007
IEEE Instrumentation & Measurement Technology
Conference IMTC 2007, 1–5,
doi: 10.1109/IMTC.2007.379183

Rodríguez Gómez, J. M., Palacios, J., Vieira, L. E. A., &
Dal Lago, A. 2019, ApJ, 884, 88,
doi: 10.3847/1538-4357/ab40af

Roša, D., Vršnak, B., Božić, H., et al. 1998, SoPh, 179, 237,
doi: 10.1023/A:1005035213782

Ruždjak, D., Brajša, R., Sudar, D., Skokić, I., & Poljančić
Beljan, I. 2017, SoPh, 292, 179,
doi: 10.1007/s11207-017-1199-8

Ruždjak, D., Ruždjak, V., Brajša, R., & Wöhl, H. 2004,
SoPh, 221, 225,
doi: 10.1023/B:SOLA.0000035066.96031.4f

Schröter, E. H., Wöhl, H., Soltau, D., & Vázquez, M. 1978,
Solar Physics, 60, 181,
doi: 10.1007/BF00152342/METRICS

Sharma, J., Kumar, B., Malik, A. K., & Vats, H. O. 2020,
Monthly Notices of the Royal Astronomical Society, 492,
5391, doi: 10.1093/mnras/staa188

Sharma, J., Kumar, B., Malik, A. K., & Vats, H. O. 2021,
Monthly Notices of the Royal Astronomical Society, 506,
4952, doi: 10.1093/MNRAS/STAB1959

Sime, D. G., High, R. R. F., & Altrock, R. C. 1989, ApJ,
336, 454, doi: 10.1086/167024

Simon, G. W., Noyes, R. W., Simon, G. W., & Noyes,
R. W. 1972, SoPh, 22, 450, doi: 10.1007/BF00148710

Simon, G. W., Seagraves, P. H., Tousey, R., et al. 1974,
SoPh, 39, 121, doi: 10.1007/BF00154974

Snodgrass, H. B. 1983, ApJ, 270, 288, doi: 10.1086/161121

—. 1984, SoPh, 94, 13, doi: 10.1007/BF00154804

Snodgrass, H. B. 1992, in Astronomical Society of the
Pacific Conference Series, Vol. 27, The Solar Cycle, ed.
K. L. Harvey, 71

Snodgrass, H. B., College, C., & Ulrich, R. K. 1990, The
    Astrophysical Journal, 3093, 309

Solanki, S. K. 1993, SSRv, 63, 1, doi: 10.1007/BF00749277

Stenflo, J. O. 1989, A&A Rv, 1, 3, doi: 10.1007/BF00872483

Stix, M. 1976, A&A, 47, 243

Sudar, D., Skokić, I., Brajša, R., & Saar, S. H. 2015,
    Astronomy & Astrophysics, 575, A63,
    doi: 10.1051/0004-6361/201424929

Ternullo, M. 1986, Solar Physics, 105, 197,
    doi: 10.1007/BF00156387

Ulrich, R. K., & Bertello, L. 1996, ApJL, 465, L65,
    doi: 10.1086/310121

Vats, H. O., Cecatto, J. R., Mehta, M., Sawant, H. S., &
    Neri, J. A. C. F. 2001, The Astrophysical Journal, 548,
    L87, doi: 10.1086/318924

Vats, H. O., Deshpande, M. R., Shah, C. R., & Mehta, M.
    1998, SoPh, 181, 351, doi: 10.1023/A:1005070616574

Vernazza, J. E., Avrett, E. H., & Loeser, R. 1981, ApJS,
    45, 635, doi: 10.1086/190731

Vršnak, B., Roša, D., Božić, H., et al. 1999, SoPh, 185, 207,
    doi: 10.1023/A:1005107424355

Wang, Y. M., Nash, A. G., & Sheeley, N. R., J. 1989,
    Science, 245, 712, doi: 10.1126/science.245.4919.712

Wang, Y. M., Sheeley, N. R., J., Nash, A. G., & Shampine,
    L. R. 1988, ApJ, 327, 427, doi: 10.1086/166205

Ward, F. 1966, ApJ, 145, 416, doi: 10.1086/148783

Weber, E. J. 1969, SoPh, 9, 150, doi: 10.1007/BF00145735

Weber, M. A. 1999, PhD thesis, Montana State University,
    Bozeman

Weber, M. A., Acton, L. W., Alexander, D., Kubo, S., &
    Hara, H. 1999, Solar Physics, 189, 271,
    doi: 10.1023/A:1005243924098

Xiang, N. B., Qu, Z. N., & Zhai, Q. 2014, AJ, 148, 12,
    doi: 10.1088/0004-6256/148/1/12

Xie, J. L., Shi, X. J., & Zhang, J. 2017, The Astrophysical
    Journal, 841, 42, doi: 10.3847/1538-4357/aa6d7d

Xu, J. C., & Gao, P. X. 2016, ApJ, 833, 144,
    doi: 10.3847/1538-4357/833/2/144

Zaatri, A., Wöhl, H., Roth, M., Corbard, T., & Brajša, R.
    2009, A&A, 504, 589, doi: 10.1051/0004-6361/200912130

Zhang, X., Deng, L., Fei, Y., Li, C., & Tian, X. 2023, The
    Astrophysical Journal Letters, 951, L3,
    doi: 10.3847/2041-8213/ACD9A3